atmosphere

MDPI

Article

Investigation of the North Atlantic Oscillation and Indian Ocean Dipole Influence on Precipitation in Turkey with Cross-Spectral Analysis

Umut Sakine Demir * and Abdullah Cem Koc

Civil Engineering Department, Pamukkale University, Denizli 20160, Turkey; a_c_koc@pau.edu.tr
* Correspondence: udemir@pau.edu.tr; Tel.: +90-258-2963359

Abstract: Predicting the future behavior of precipitation is of the utmost importance for planning agriculture or water resource management and in designing water structures. Determining the relationships between precipitation and the oceans may enable more accurate predictions. Therefore, oceanic and other persistent indices called teleconnection patterns can be used, namely the North Atlantic oscillation (NAO) and the Indian Ocean dipole (IOD). The NAO affects the precipitation patterns in the Atlantic Ocean and Mediterranean countries, such as in Turkey. The IOD is related to temperature and precipitation in the Indian Ocean coastal countries and in some areas far from the Indian Ocean. In this study, the effects of the NAO and IOD indices on precipitation in Turkey were investigated by means of cross-spectral analysis between the monthly total precipitation (mm) and monthly NAO and IOD index values. Phase shift values were also calculated for the selected periods and their accuracy was evaluated statistically, using the determination coefficient (R^2) and Akaike information criterion (AIC) as performance criteria for the linear model. The results indicated strong correlations for the 13-, 14-, 16-, and 22–23-month periods between the NAO index and precipitation values; and for the 13-, 14-, 16–17-, and 20–21-month periods between the IOD index and precipitation values. After cross-spectral analysis between the NAO and IOD indices and precipitation values, the maximum phase shift values increased as the periods increased, while the maximum phase shift value for each period was almost half of the period value. Moreover, the maximum cross-power spectral density (CPSD) values increased as the periods increased. High CPSD values were observed in the west of Turkey for the NAO and in the east of Turkey for the IOD.

Keywords: NAO; IOD; precipitation; cross-spectral analysis; Turkey

Citation: Demir, U.S.; Koc, A.C. Investigation of the North Atlantic Oscillation and Indian Ocean Dipole Influence on Precipitation in Turkey with Cross-Spectral Analysis. *Atmosphere* **2021**, *12*, 99. https://doi.org/10.3390/atmos12010099

Received: 27 October 2020
Accepted: 5 January 2021
Published: 12 January 2021

1. Introduction

Precipitation is one of the most important components of the hydrological cycle; it also affects other components such as flow, infiltration, and evaporation. Forecasting future precipitation behavior is important for planning agriculture or water resource management and in designing water structures. The winter and spring precipitation are cyclonic precipitation in Turkey which are more associated with the ocean oscillation. Summer precipitation is convectional and occur with the air rising during the day. Precipitation is highly variable both spatially and temporally in Turkey. Therefore, precipitation prediction is very difficult. Atmospheric physics and climatic processes are important for prediction of precipitation in Turkey. Short-term precipitation forecasting models such as European Centre for Medium-Range Weather Forecasts (ECMWF ERA5), Weather Research and Forecasting (WRF), ALadin and AROme (ALARO), Climate Forecast System (CFS) and Global Forecast System (GFS) are used to prediction of Turkey's precipitation. However, the verification and comparison of these models has been not carried out for entire Turkey so far. The studies were performed usually for single model, limited region, very short term events, and not for all months. Oceans play an important role in the Earth's climate, so determining the relationships between precipitation and the climate indicators related to

the oceans may enable more accurate precipitation forecasts. The climate indicators related to the oceans are called oceanic oscillations because of their periodic behavior. The physical links between ocean oscillations and precipitation may be explained as follows. Pressure or temperature differences on the oceans' surfaces cause the movement of air masses. The movement of air masses determine in which regions precipitation will occur. For example, the sea level pressure differences between the north and the center of the Atlantic Ocean, (the North Atlantic oscillation—NAO), cause movements of air masses in north and south directions. Sea surface temperature differences (Indian Ocean dipole—IOD) between the east and west of the Indian Ocean cause the movement of air masses in the east and west directions. Since the beginning of the 20th century, researchers have investigated the relationships between low-frequency fluctuations in atmospheric circulation and weather patterns [1]. Because of the transient behavior of atmospheric planetary-scale waves, simultaneous changes occur at very different points on earth. These simultaneous changes in climate are commonly referred to as "teleconnections" in the meteorology literature [2]. Teleconnections can comprise a basis for long-term climate forecasts [1].

While Walker [3] was researching the Indian monsoon rainfall forecasts, he noticed that the time series of mean sea level pressure and surface air temperature data during the winter at stations in North America and Europe were strongly correlated with each other. He realized that this strong correlation was a reflection of planetary-scale fluctuations, which he termed the North Atlantic oscillation (NAO) [3–5]. The NAO is associated with changing westerlies from the Northern Atlantic to Europe [6]. The NAO is the most prominent and recurrent pattern of atmospheric variability in the middle and high latitudes of the Northern Hemisphere, especially during the cold season (November–April). The NAO determines climate variability from the East Coast of the United States to Siberia and from the Arctic to the subtropical Atlantic, especially during the winter months; therefore, changes in the NAO are important to society and the environment [7]. The NAO has the greatest impact on precipitation in Western Europe and it increases precipitation from the British Isles to Scandinavia [8]. Rain occurs in Europe during the positive phase of the NAO, while heavy rainfall occurs in the Mediterranean basin during its negative phase [9]. Dry wintertime conditions in Southern Europe and the Mediterranean and wetter than normal conditions in Northern Europe and Scandinavia since 1980 are also linked to the NAO's behavior [10]. The NAO index represents information about temperature, storms, precipitation, cloudiness, hydrographic characteristics, mixed-layer depths, and circulation patterns in the ocean [2]. The relationship between precipitation and the NAO has previously been investigated in the East Coast of United States [1], Italy [11], Morocco [12], Spain [13,14], and France [15,16], among other. These studies proved the relationship between the NAO and precipitation in the Atlantic coast and Mediterranean basin countries. The findings and results for some of these studies are as follows. Castro et al. [13] investigated the effect of the NAO on precipitation in Spain. They established simple and multiple linear regression models using monthly, seasonal, and annual precipitation data and the corresponding NAO index values to predict precipitation. They showed that the NAO index may be used for forecasting seasonal precipitation, especially fall precipitation. Garcia et al. [14] showed the relationships between precipitation in Galicia, Spain, and the NAO index at 8 years period using singular spectrum analysis.

On the other hand, predictions of the NAO are useful for the economy and environment, and therefore several dedicated forecasting methods and services have been developed. Based on the principal components of sea surface temperature (SST) changes, Saunders and Qian [17] improved an empirical model to predict winter NAO index. Eshel [18] used the North Pacific surface pressure to produce 21-month forecasts of NAO based on various autoregressive models. Recently, Wang et al. [19] developed a new empirical model which is skillful empirical model using multiple linear regression (MLR) to predict winter NAO variability. Dobrynin et al. [20] used a dynamical ensemble model to produce seasonal NAO forecasts. Lastly, Chlaściak and Niedzielski [21] proposed a new approach for forecasting the NAO index based on predictions of sea level anomalies

(SLAs). One of the main results of the study is that it is possible to produce long-term (up to 3-months) predictions of the NAO index based solely on SLAs. As seen in the literature, predicting to NAO index and validation of prediction is important issue. New approaches must be capable of make both the future prediction of the NAO index and verify it with historical data. Therefore, this study may be a method for making these verifications.

Saji et al. [22] developed a dipole mode index called the Indian Ocean dipole (IOD), which causes interannual climate change in the tropical Indian Ocean. This pattern has internal variability with anomalously low sea surface temperatures off Sumatra and high sea surface temperatures in the Western Indian Ocean [22]. The IOD contains two large-scale, distinct anomaly patterns that are related to temperature and precipitation in the Indian Ocean coastal countries. In the first pattern, land temperatures and precipitation are abnormally high in the countries on the western coast of the Indian Ocean, while abnormally they are low on the eastern coast. In the second pattern, Asian monsoon rain increases and extends from Pakistan to southern China. In addition, the IOD effects are also seen in some areas far from the Indian Ocean. The IOD events also affect Europe, northeast Asia, North and South America, and South Africa. Positive IOD values correlate with warm land surfaces and decreasing precipitation in these regions [23].

There are many studies in the literature showing that the IOD affects precipitation in America, Europe, Africa and Asia, East Africa and Indonesia [22,24], Ethiopia [25], East Asia [26], Asia [27], Pakistan [28], Australia and Brazil [29], Europe [30], and South America [29,31]. From these studies, Hussein et al. [28] investigated the relationship between the Indian Ocean dipole (IOD) and precipitation in Pakistan using data from 1958–2010. They found a significant positive correlation between the IOD index and annual and summer precipitation.

Turkey is situated in the Northern Hemisphere in the eastern Mediterranean region, which is the impact zone for maritime and continental air masses. In the winter season, maritime polar air masses from the North Atlantic Ocean and continental polar air masses from Siberia occur; in the summer season, the maritime air masses from the Central Atlantic Ocean (Azores) and continental tropical air masses from the North Africa constitute rainfall occur [32]. Precipitation in Turkey is usually associated with the activities of the above-mentioned air masses, except for the convectional precipitation in summer [33]. In parallel to the above studies, the relationships between the NAO index, precipitation, and other climate parameters in Turkey have also been investigated by numerous studies [33–41]. Some of these studies have indicated that winter precipitation regimes in western and central Turkey are substantially influenced by the NAO [33,34]. From these studies, Türkeş and Erlat [34] investigated the effect of the NAO on precipitation in Turkey. For this purpose, monthly total precipitation data from 78 stations in Turkey for the period 1930–2000 were used. They found a negative relationship between the NAO index and precipitation. Spatially coherent and statistically significant changes in precipitation were more evident in western and central Turkey for extreme NAO phases.

Turkey is divided into seven rainfall regions in terms of the percentages of seasonal rainfall versus the annual rainfall total, as shown in Figure 1 [33]. The Köppen–Geiger climate classification for Turkey is given in Figure 2 [42]. Accordingly, there are 13 different climate regions in Turkey.

The aim of this study is investigating the influences of the NAO and the IOD on precipitation in Turkey through cross-spectral analysis. For this purpose, 239 stations were considered, which are located in different regions of Turkey. We also checked the phase shift values obtained after the cross-spectral analysis by means of performance criteria from linear models. This paper consists of four sections. In Section 2, the data description and method explanation are provided. Results for the linkages between teleconnection patterns and precipitation are given in Section 3 and the statistical model is presented. The last part, Section 4, is devoted to the conclusions. The temporal variations of monthly total precipitation and monthly NAO and IOD index values are periodic signals consisting of many different frequencies, besides including trends and noise. Since the signals are

periodic, they are studied in the frequency domain instead of the time domain. A general flow chart of this study is given in Figure 3.

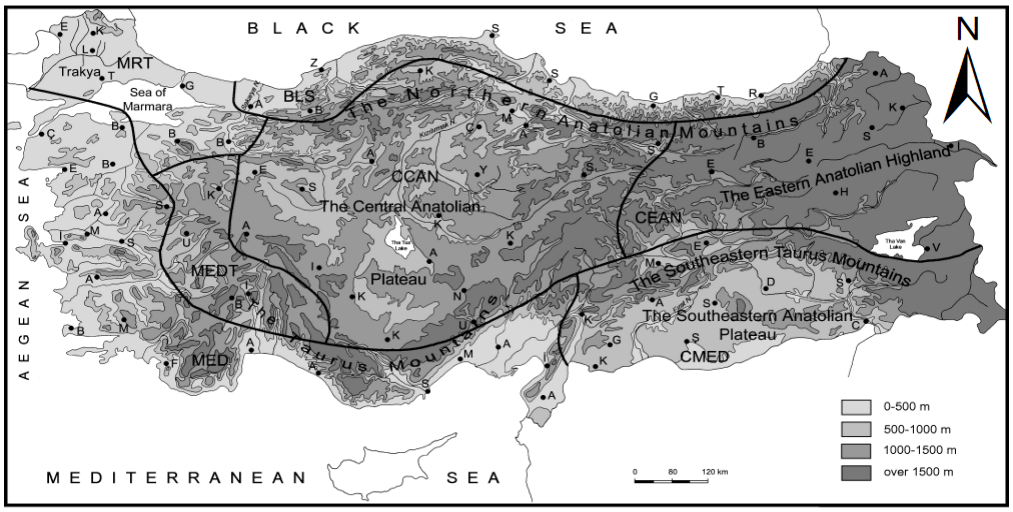

Figure 1. Rainfall regions of Turkey shown over on a physical map. The dots are locations of the meteorology stations, along with first letter of each station name. BLS: Black Sea; MRT: Marmara Transition; MED: Mediterranean; MEDT: Mediterranean Transition; CMED: Continental Mediterranean; CCAN: Continental Central Anatolia; CEAN: Continental Eastern Anatolia [33].

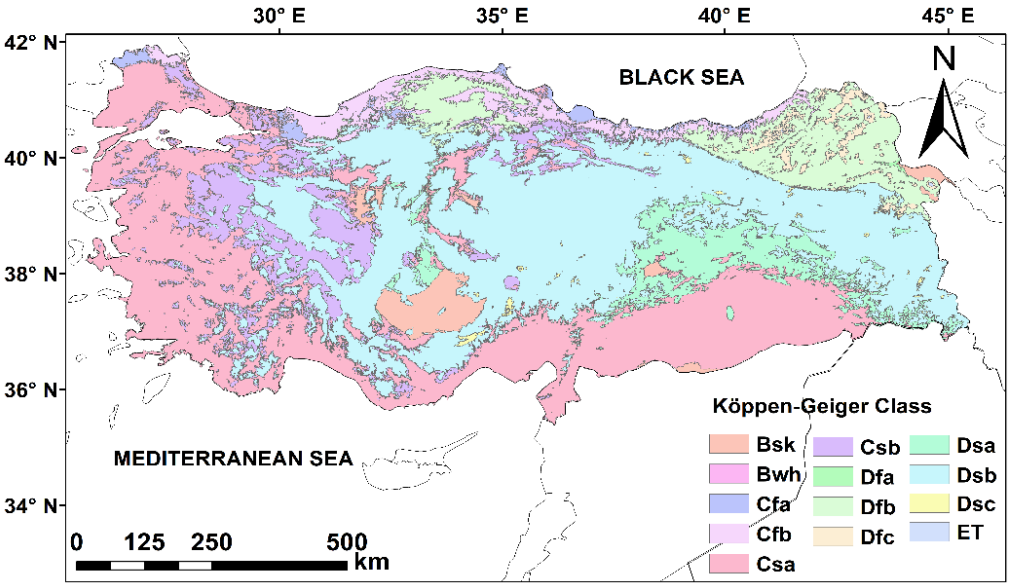

Figure 2. The Köppen–Geiger climate classification for Turkey. BSk: arid steppe cold; Bwh: arid desert hot; Cfa: temperate without dry season, hot summer; Cfb: temperate without dry season, warm summer; Csa: temperate, dry summer, hot summer; Csb: temperate, dry summer, warm summer; Dfa: cold without dry season, hot summer; Dfb: cold without dry season, warm summer; Dfc: cold without dry season, cold summer; Dsa: cold, dry summer, hot summer; Dsb: cold dry season warm summer; Dsc: cold, dry season, cold summer; ET: polar tundra [42].

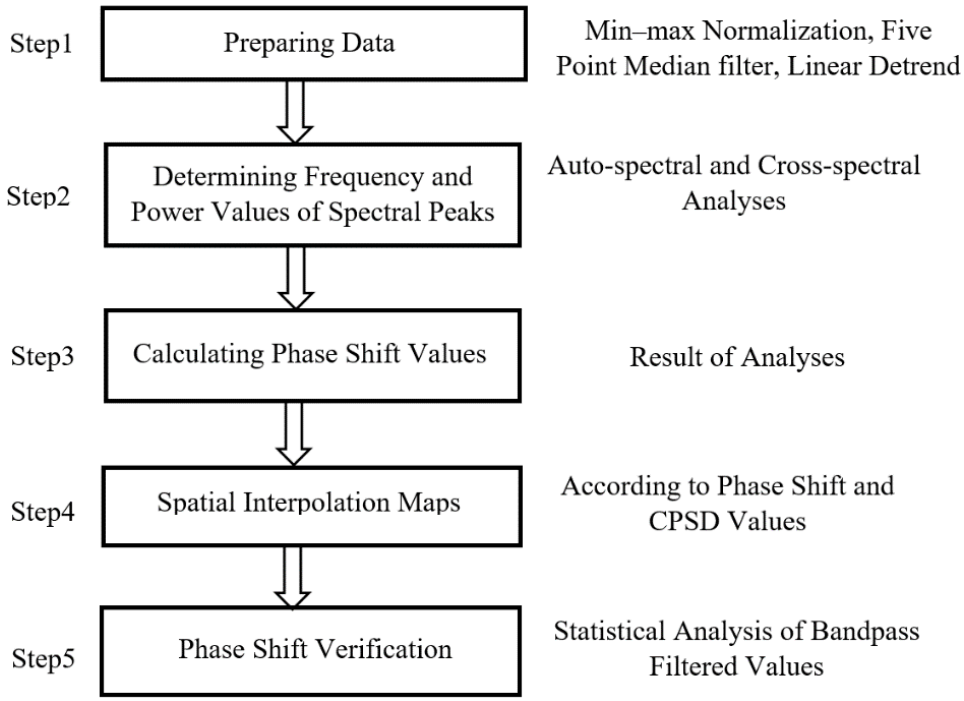

Figure 3. General flow chart for this study.

2. Material and Method

Monthly total precipitation (mm) and monthly NAO and IOD index values are the data used in this study. Auto-spectral and cross-spectral analyses were applied and the base periods and phase shifts of the data were determined. Min–max normalization was performed on the precipitation data and the NAO and IOD index values before the analyses. Before the auto-spectral analysis, five-point median filter and linear detrending processes were applied to the normalized index values, whereas only linear detrending was performed for the normalized precipitation data. The sea level pressure values used for the calculation of the NAO index are significantly affected by small-scale and transient meteorological events not related to the NAO, and therefore contain noise [2]. For this reason, a five-point median filter was applied to index values. Before the cross-spectral analysis, five-point median filter and linear detrending processes were applied to both the normalized indices and normalized precipitation data.

2.1. Meteorology Stations and Precipitation Data

In this study, 239 Turkish State Meteorological Service meteorology stations containing uninterrupted monthly total precipitation (mm) data for a length of at least 30 years from across the different regions of Turkey were used. Later in this paper, analysis results are examined in detail for Bodrum and Igdir meteorology stations (Figure 4). Precipitation measurements for the Bodrum station were started in 1938 (Figure 5) and for Igdir station in 1957 (Figure 6); values up to the end of 2017 were used in this study for both stations. Before the analyses, the monthly total precipitation height (P_i) values for each station were brought to the range of 0 to 1 (Pn_i) by performing min–max normalization (Equation (1)).

$$Pn_i = \frac{P_i - P_{min}}{P_{max} - P_{min}} \quad (1)$$

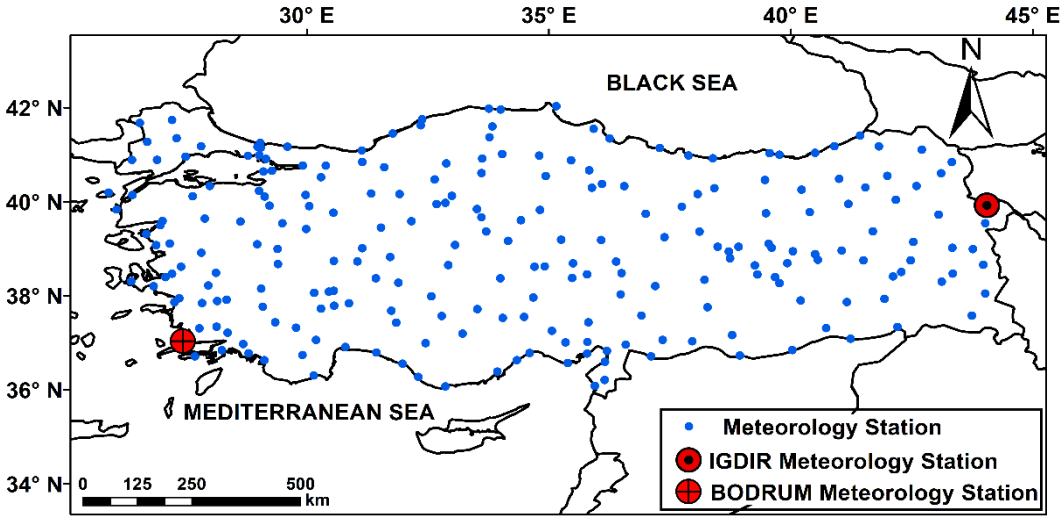

Figure 4. The meteorology stations considered in this study.

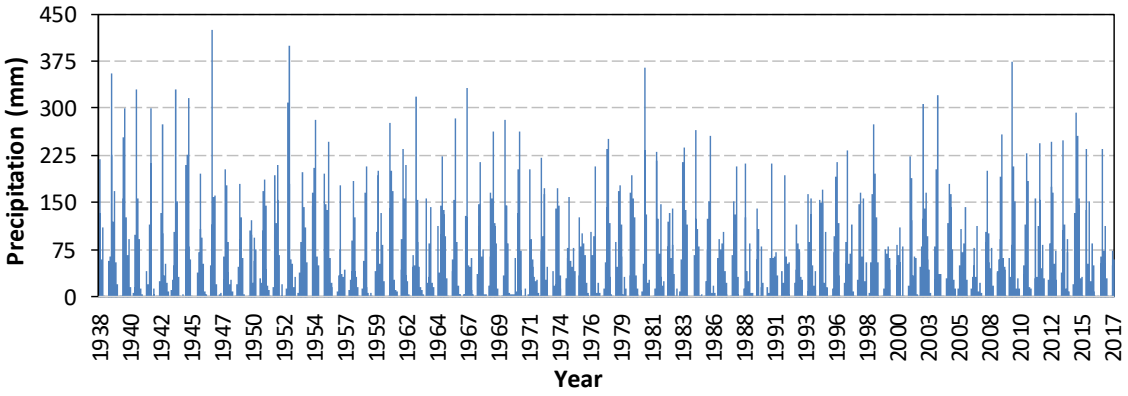

Figure 5. Monthly total precipitation (mm) data for Bodrum meteorology station.

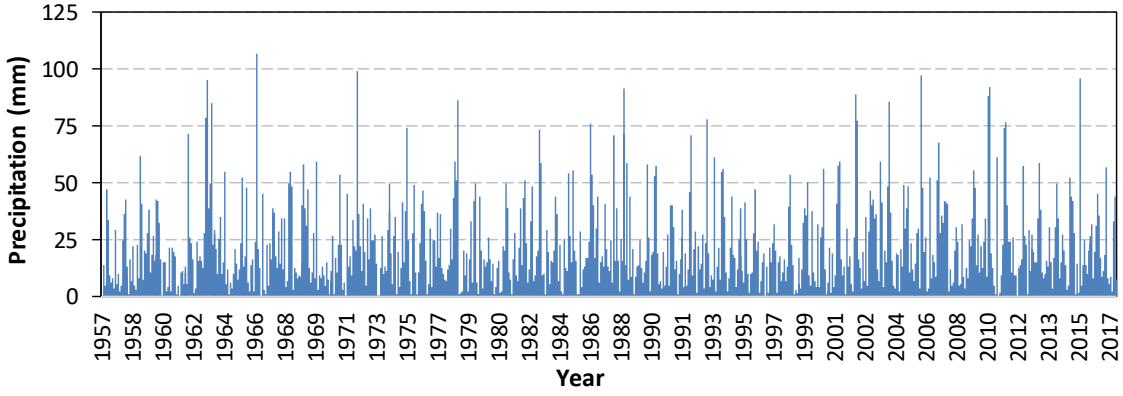

Figure 6. Monthly total precipitation (mm) data for Igdir meteorology station.

2.2. NAO Data

The NAO indices are calculated by using normalized sea level pressure (SLP) differences from a northern and a central Atlantic station. Some common station couples are Ponta Delgada (Azores) and Stykkisholmur (Reykjavik, Iceland); Lisbon (Portugal) and Stykkisholmur (Reykjavik, Iceland); and Gibraltar (Iberian Peninsula) and Reykjavik (Iceland) [43]. The monthly NAO index data from between 1865 and 2017 used in this study were calculated by subtracting the normalized sea level pressure (SLP) values of

Stykkisholmur (northern station) from the Ponta Delgada (southern station) values [44], which are given in Figure 7. Before the analyses, the NAO index values were brought between 0 and 1 by performing min–max normalization (Equation (2)).

$$NAOn_i = \frac{NAO_i - NAO_{min}}{NAO_{max} - NAO_{min}} \quad (2)$$

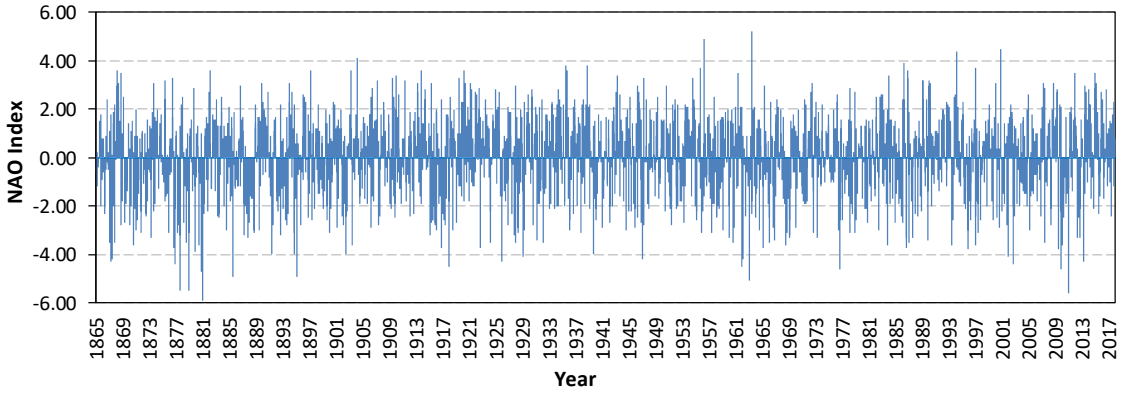

Figure 7. The monthly NAO index values for the period 1865−2017.

2.3. IOD Data

The monthly IOD index data for between 1870 and 2017 used in this study were calculated by subtracting the southeastern Indian Ocean sea surface temperature anomaly (SSTA) (90°–110° E, 10°–0° S) values from western Indian Ocean sea surface temperature anomaly (50°–70° E, 10°S–10° N) values [22,45], which are given in Figure 8. Before the analyses, the IOD index values were brought in between 0 and 1 by performing min–max normalization (Equation (3)).

$$IODn_i = \frac{IOD_i - IOD_{min}}{IOD_{max} - IOD_{min}} \quad (3)$$

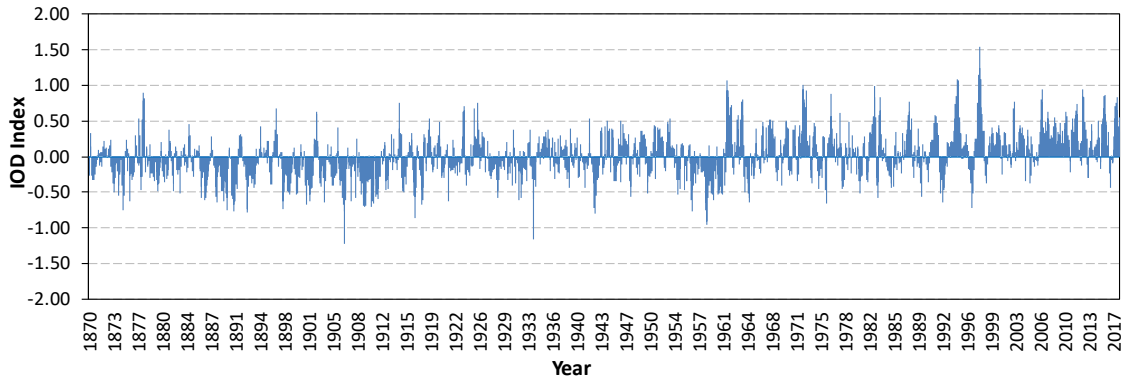

Figure 8. The monthly Indian Ocean dipole (IOD) index values for the period 1870−2017.

2.4. Auto-Spectral and Cross-Spectral Analysis

Auto-spectral analysis describes the distribution of variance in one single time series signal over a frequency or wavelength. The power spectrum of a time series shows the distribution of power into frequency components of the signal. A common method used to calculate the power spectrum is the periodogram method, which is a special case of the

method used by Blackman and Tukey [46]. A periodogram is a nonparametric estimate of the power spectral density of a stationary random process. A periodogram is a Fourier transform of the biased estimate of the autocorrelation sequence and is calculated as in the Equation (4).

$$\hat{P}(f) = \frac{\Delta t}{N}\left|\sum_{n=0}^{N-1} x_n e^{-j2\pi f \Delta t n}\right|^2, \frac{-1}{2\Delta t} < f < \frac{1}{2\Delta t} \quad (4)$$

where $\hat{P}$ is the power spectral density, Δt is the sampling interval, f is the frequency, and N is the number of data points. Computation of the power spectrum can only be performed at a limited number of frequencies using a fast Fourier transform (FFT). An FFT is a method used for computing a discrete Fourier transform, which is an approximation of the continuous Fourier transform in a short time. Most FFT algorithms divide the transformation into two pieces of size $N/2$ at each step. Hence, the dimensions of the transformation are equal to the power of two. The spectrum is calculated using the frequency close to the number of data points in the original x signal [47].

Cross-spectral analysis relates two-time series in the frequency domain (Equations (5) and (6)).

$$P_{xy}(w) = \sum_{m=-\infty}^{\infty} R_{xy}(m) e^{-jwm} \quad (5)$$

$$R_{xy}(m) = E\{x_{n+m} y_n^*\} = E\{x_n y_{n-m}^*\} \quad (6)$$

where P_{xy} is the cross-spectral power density containing amplitude and phase information for x and y time series, $R_{xy}(m)$ is the cross-correlation sequence, and E is the expected value.

3. Results and Discussion

After auto-spectral analysis, power spectral densities were obtained for the NAO and IOD indices (Figure 9) and for monthly total precipitation data. Power spectral density graphs for the Bodrum and Igdir meteorology stations are given in Figure 10.

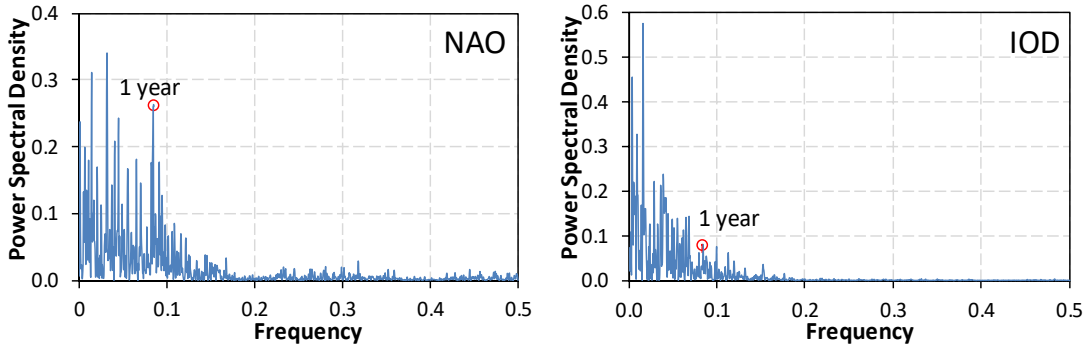

Figure 9. Auto-spectral analysis results for the monthly North Atlantic oscillation (NAO) and IOD indices.

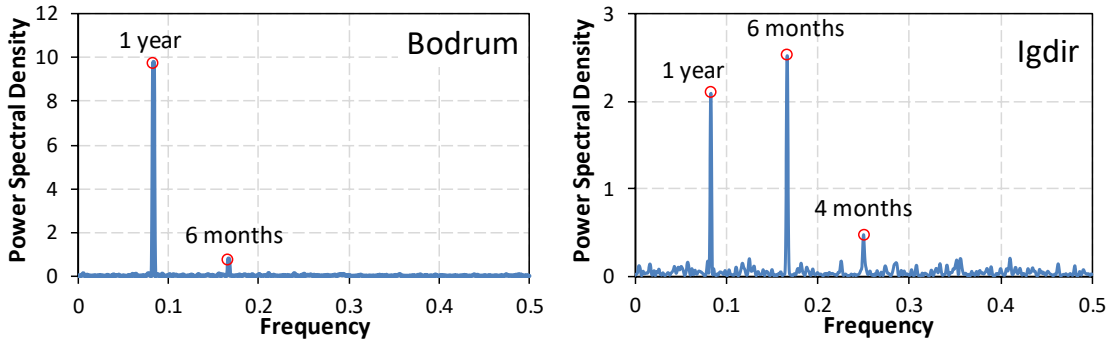

Figure 10. Auto-spectral analysis results for monthly total precipitation at Bodrum and Igdir stations.

As expected, strong power spectral density values can be observed for periods longer than 1 year (frequencies smaller than 0.083) in the power spectral density graphs of the NAO and IOD indices (Figure 9). On the contrary, again as expected, strong power spectral density values can be observed for periods of 1 year or shorter (frequencies greater than 0.083) in the power spectral density graphs of the monthly total precipitation.

As expected, the strongest power spectral density value can be observed for the annual period (frequency = 0.083) in the power spectral density graph for the Bodrum meteorology station, while the second strongest power spectral density value is at the frequency of 0.167, corresponding to the 6-month period. The power spectral density values of the other periods are negligible. For Igdir meteorology station, the strongest power spectral density value can be observed for the semiannual period (frequency = 0.167) in the power spectral density graph. Other strong power spectral density values can be seen at the frequencies of 0.083 and 0.25, corresponding to the 12- and 4-month periods, respectively (Figure 10).

Generally, according to the power spectral density values, dominant periods for monthly total precipitation in Turkey are 12, 6, and 3 months. Power spectral density values at frequencies corresponding to periods greater than 1 year are very weak compared to the dominant periods.

Normalized, five-point median-filtered, and detrended monthly total precipitation values for the meteorology stations with the NAO and IOD indices were used in the cross-spectral analysis. CPSD graphs of Bodrum-NAO and Igdir-IOD after cross-spectral analysis are given in Figure 11.

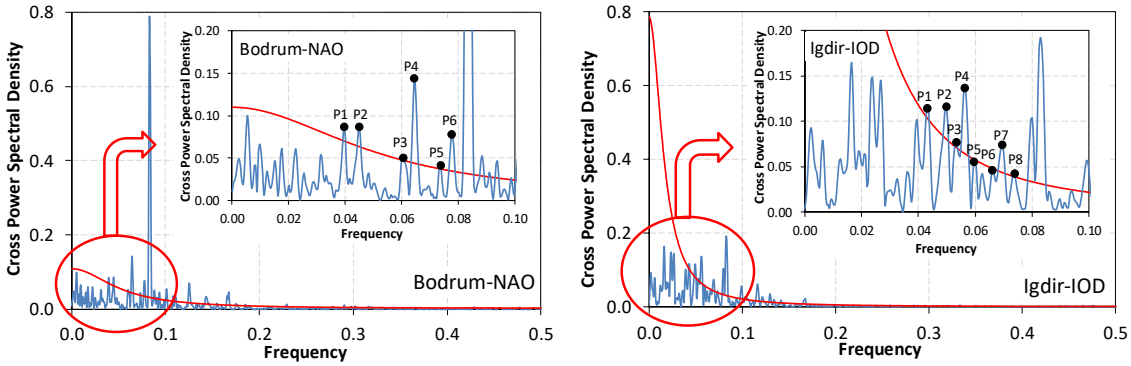

Figure 11. Cross-spectral analysis results of Bodrum-NAO and Igdir-IOD with red noise.

The red lines in Figure 11 represent the red noise. A red noise line is drawn to determine the noise that may reach the CPSD values even after the median filter. Red noise is used to describe various types of noise, including low-frequency fluctuations from the interactions of white noise with the slow-response components of the system. There is also notable empirical evidence that the red noise model provides a reasonable description of the noise spectra for various climatic and hydrological time series, including long-term climate records [48], historical sea and air surface temperature data [49,50], and station precipitation data [51,52]. The red noise spectrum is defined by the spectral density of the first order autoregressive AR (1) model [53]. The power spectrum of the AR 1 model is given in Equation (7) [54].

$$S(f) = S_0 \frac{1 - r^2}{1 - 2rcos\left(\frac{2\pi f}{f_N}\right) + r^2} \quad (7)$$

where $S_0 = \frac{\sigma^2}{1-r^2} \geq 0$ is the average value of the power spectrum; r is the lag-1 autocorrelation; $f_N = \frac{1}{\Delta t}$ is the Nyquist frequency; Δt is the sampling interval; f is the frequency; σ^2 is the variance of the time series.

In the cross-spectral analysis, peaks corresponding to periods 1 year and shorter having frequency values greater than 0.083 were not taken into account, since a 5-point median filter was applied to precipitation and index values. The cross-spectral analysis graphs were examined in detail. In Figure 11 for Bodrum-NAO and Igdir-IOD, the peaks were not taken into account, which are below the red noise line. The frequencies, periods (months), CPSD values, and phase shift (Months) of the peaks are given in Table 1.

Table 1. Frequency, period, cross-power spectral density (CPSD), and phase shift values of the peaks from Figure 11.

Bodrum-NAO					Igdir-IOD				
Peak Num	**Frequency**	**Period**	**CPSD**	**Phase Shift**	**Peak Num**	**Frequency**	**Period**	**CPSD**	**Phase Shift**
P1	0.039551	25	0.086702	6	P1	0.043457	23	0.117002	−5
P2	0.044922	22	0.087209	−8	P2	0.049805	20	0.116221	−4
P3	0.060059	17	0.053597	3	P3	0.053223	19	0.076957	1
P4	0.064453	16	0.143938	−7	P4	0.056152	18	0.136801	3
P5	0.073242	14	0.045073	−6	P5	0.060059	17	0.058649	−5
P6	0.077637	13	0.078003	−5	P6	0.066406	15	0.046864	2
					P7	0.069336	14	0.074182	−3
					P8	0.073730	14	0.042564	4

In Table 1, negative phase shift values show the leading cases for the NAO and IOD indices. Similarly, the same procedures were performed for all meteorological stations and the numbers of stations in the periods with negative phase shifts were obtained.

Analyses were repeated with the removing harmonics that are periodic with the annual cycle. For this purpose, min–max normalization and linear detrend were applied to the NAO, IOD, Bodrum and Igdir data. The climatological average of the harmonics that are periodic with the annual cycle were removed and to see the effect of removed harmonics, 5-point median filter was not performed. Then cross spectral analyses were repeated for Bodrum-NAO and Igdir-IOD Figure 12. Frequency values in Figure 12 are shown between 0 and 0.1 in order to compare them with the peaks in Figure 11.

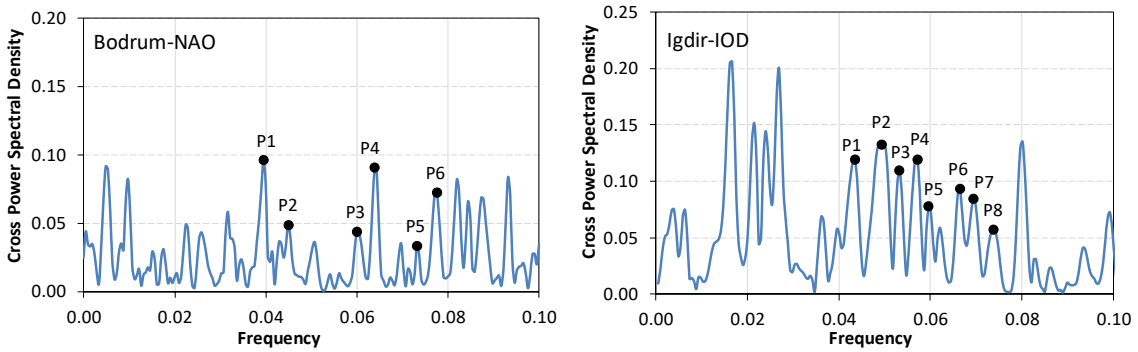

Figure 12. Cross-spectral analysis results of Bodrum-NAO and Igdir-IOD with removed harmonics.

The frequencies, periods (months), CPSD values, and phase shift (months) of the peaks for the removed harmonics were given in Table 2.

In Table 2, negative phase shift values show the leading cases for the NAO and IOD indices. Similar periods were found with the values in Table 1 for both Bodrum-NAO and Igdir-IOD, and the same or maximum of 1-month different phase shift values were observed. In the next steps of the study, the results obtained with non-removed harmonics will be taken into consideration.

Table 2. Frequency, period, CPSD, and phase shift values of the peaks from Figure 12.

Bodrum-NAO					Igdir-IOD				
Peak Num	**Frequency**	**Period**	**CPSD**	**Phase Shift**	**Peak Num**	**Frequency**	**Period**	**CPSD**	**Phase Shift**
P1	0.039551	25	0.096240	5	P1	0.043457	23	0.119168	−6
P2	0.044922	22	0.048841	−7	P2	0.049805	20	0.134552	−5
P3	0.060059	17	0.043726	6	P3	0.053223	19	0.109736	3
P4	0.063965	16	0.090910	7	P4	0.056641	18	0.120374	4
P5	0.073242	14	0.033206	6	P5	0.05957	17	0.077557	−4
P6	0.077637	13	0.072500	−4	P6	0.066406	15	0.093127	3
					P7	0.069336	14	0.084341	−3
					P8	0.073730	14	0.057047	4

As a result of cross-spectral analysis between meteorology stations and the NAO and IOD indices, the CPSD, frequency, period, and phase shift values were obtained. The frequency, period, and negative phase shift values corresponding to the CPSD values above the red noise line were determined. The number of stations showing a relationship with the NAO and the IOD in periods of 13 months or longer (NAO-Stations (NAO-ST) and IOD-Stations (IOD-ST)) and average phase shift values for each period (NAO- Phase shift (NAO_PH) and IOD- Phase shift (IOD_PH)) are shown in Figure 13. In addition, coefficients of variation for phase shift values were calculated for each period (Figure 14). The periods were selected according to the number of meteorology stations correlated with the NAO and IOD indices. Periods with a large number of meteorology stations and corresponding to small phase shift coefficient of variation values were considered. Thus, 13-, 14-, 16-, and 22–23-month periods were determined for the NAO; while 13-, 14-, 16–17-, and 20–21-month periods were determined for the IOD.

Inverse-distance-weighted (IDW) spatial interpolation was performed on phase shift values and was then mapped for the NAO (Figure 15a) and IOD (Figure 15b). Similar spatial interpolations were performed for CPSD values, which were then mapped for the NAO (Figure 16a) and IOD (Figure 16b).

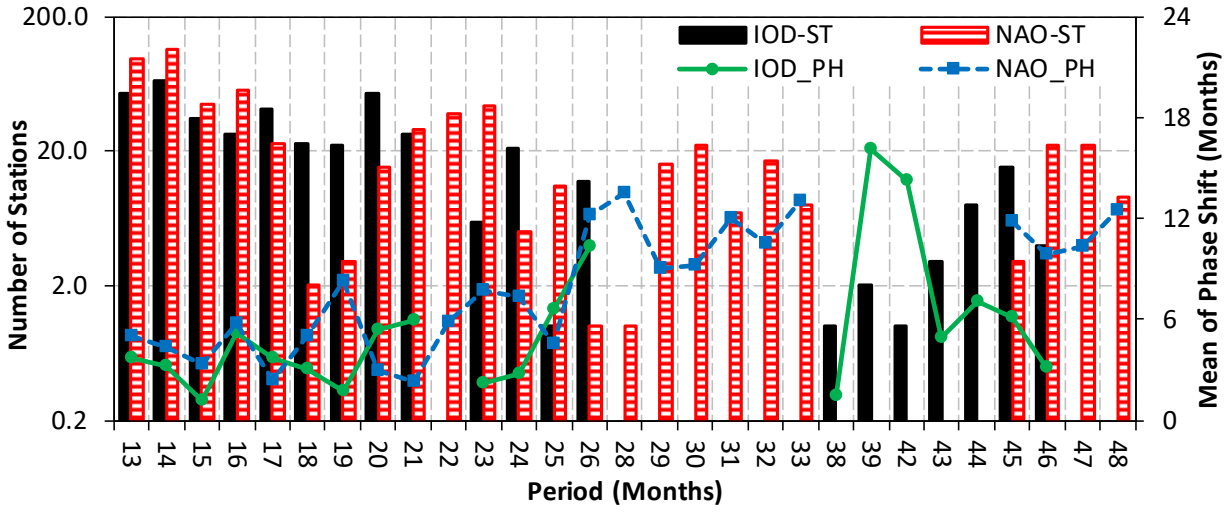

Figure 13. Numbers of stations and means of phase shift values according to the periods after the cross-spectral analyses.

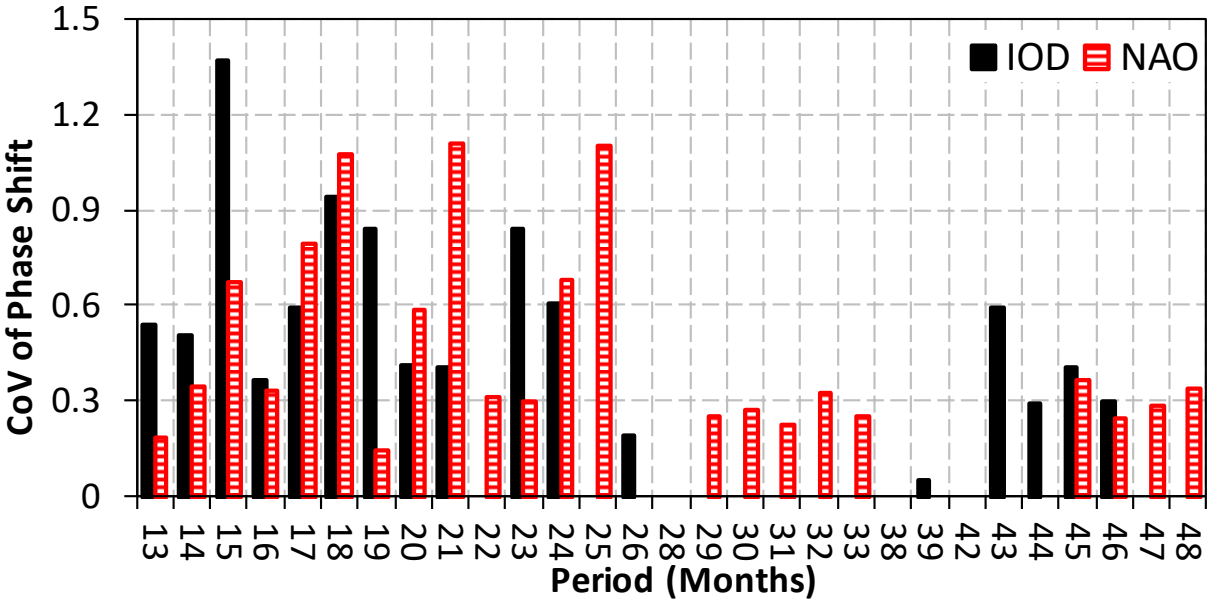

Figure 14. Coefficient of variation values for phase shifts according to the periods.

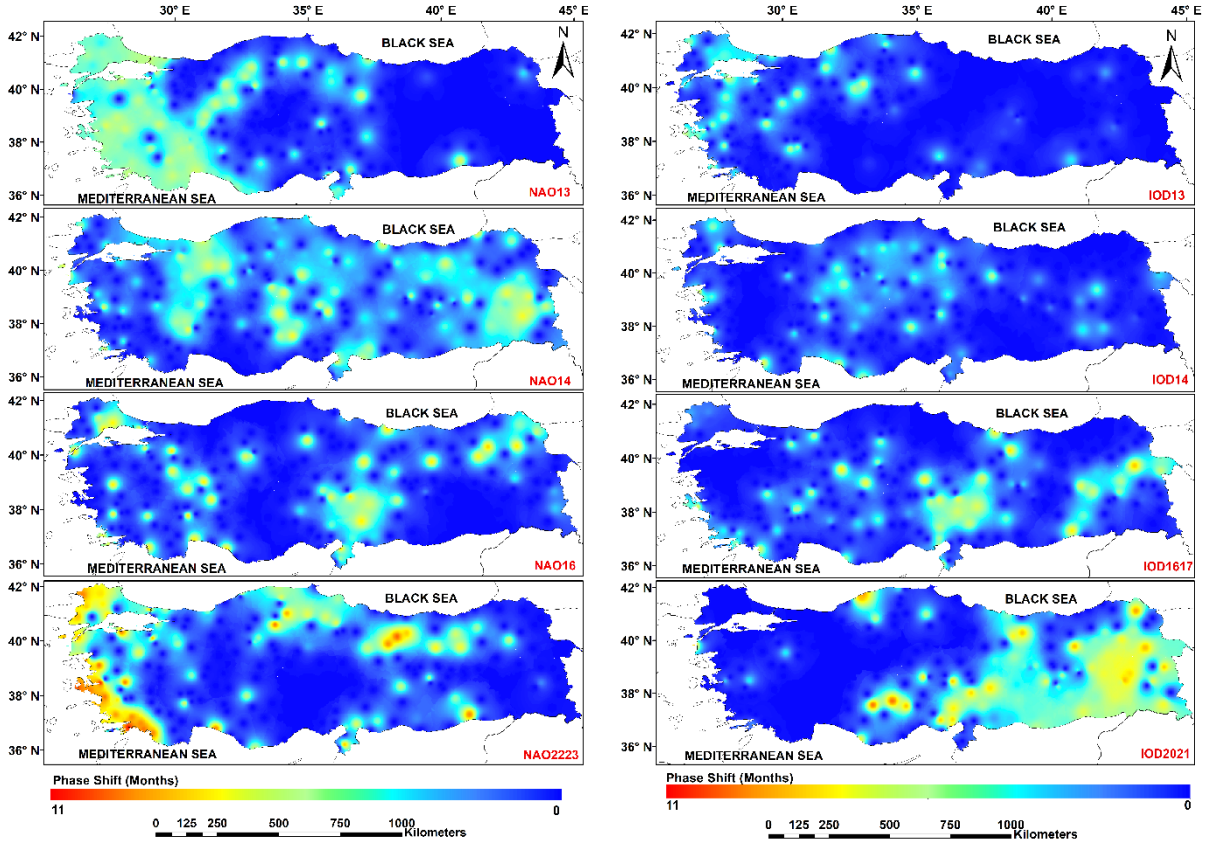

(**a**) NAO (**b**) IOD

Figure 15. Spatial distribution of phase shifts (**a**) for NAO (**b**) for IOD.

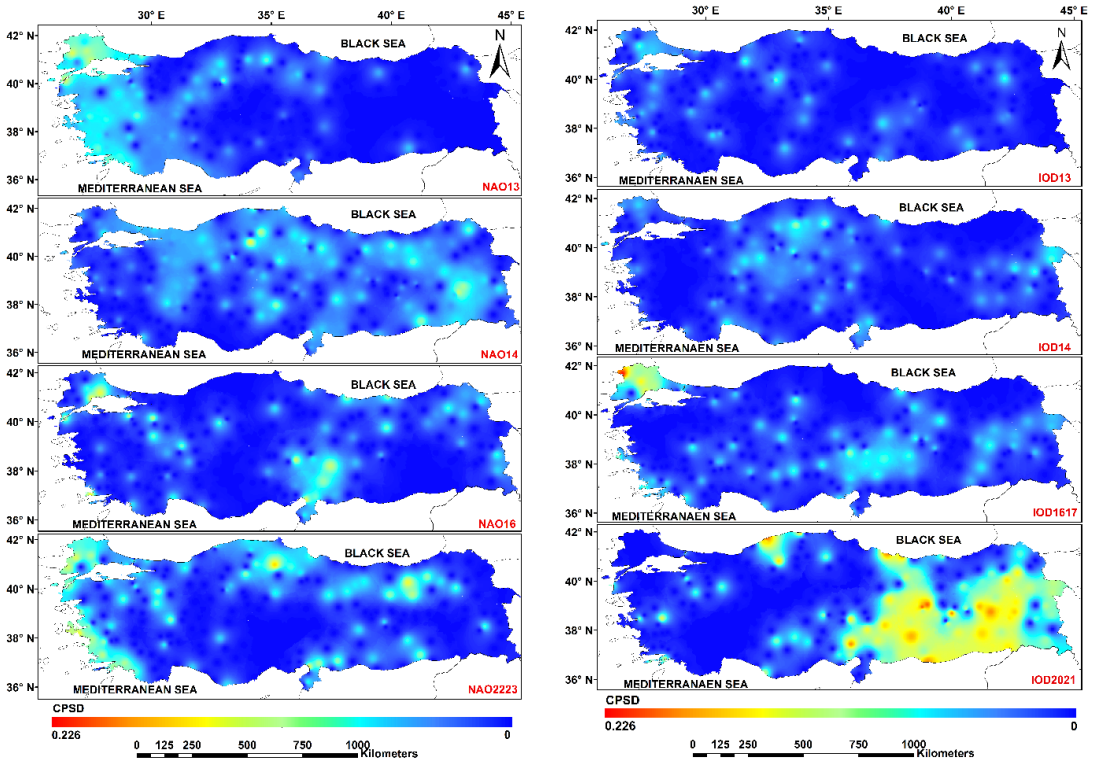

(**a**) NAO (**b**) IOD

Figure 16. Spatial distribution of CPSD values (**a**) for NAO (**b**) for IOD.

According to Figure 15a, phase shift values between the NAO and meteorology stations were clustered for the 13-month period in the west of Turkey, for the 14-month period in the inner west and east of Turkey, for the 16-month period in the south of Turkey, and for 22–23-month period in the west and north of Turkey. The phase shift values between the NAO and meteorological stations were mostly clustered in the west for the 22–23-month periods. This means that the stronger relationships were observed in the west because the Atlantic Ocean is closer to the west of Turkey.

According to the Figure 15b, phase shift values between the IOD and meteorology stations were clustered for the 13-month period in the west of Turkey, for the 14-month period in central Turkey, for the 16–17-month period in the east of Turkey, and for the 20–21-month period in the east and southeast of Turkey. On the contrary, for the NAO, the phase shift values between the IOD and meteorology stations were clustered for the 20–21-month period in the east. This means that the stronger relationships were observed in east because the Indian Ocean is closer to the east of Turkey.

For both indices, the maximum phase shift values increased as the periods increased, and the maximum phase shift value for each period was almost half of the period value (Figure 15).

According to the Figure 16a, CPSD values between the NAO and meteorology stations were clustered for the 13-month period in the west of Turkey, for the 14-month period in central and the east of Turkey, for the 16-month period in the south of Turkey, and for the 22–23-month period in the west and north of Turkey. The CPSD values between the NAO and meteorology stations were mostly clustered in the west for the 22–23-month period. This means that the stronger relationships were observed in the west because the Atlantic Ocean is closer to the west of Turkey.

According to the Figure 16b, CPSD values between the IOD and meteorology stations were clustered for the 14-month period in central Turkey, for the 16–17-month period in the east and northwest of Turkey, and for the 20–21-month period in the east and southeast of Turkey, while for the 13-month period no specific clustering was determined. In contrast

to the NAO, the CPSD values between the IOD and meteorology stations were clustered for the 20–21-month period in the east. This means that the stronger relationships were observed in the east because the Indian Ocean is closer to the east of Turkey.

For both indices, the maximum CPSD values increased as the periods increased. High CPSD values were located in the west of Turkey for the NAO and east of Turkey for the IOD (Figure 16).

The following study was carried out in order to assess the relationships between the periods and the phase shift values from another perspective. The phase shift was calculated as 7.67 months between monthly total precipitations measured at the Bodrum meteorology station and the NAO index for the 22-month period. This result indicates that the effect of the NAO is seen after 7.67 months in Bodrum meteorology station precipitation data. A 22-month band-pass filter was applied to the NAO index and the monthly total precipitation values for Bodrum meteorology station. Then, the stationarity of the band-pass-filtered series was verified with the Dickey–Fuller stationarity test [55] before performing the least squares linear regression model (Equation (8)). According to different phase shift values, the band-pass-filtered NAO index values were shifted for the relevant phase shift. Thus, the NAO leads in terms of precipitation.

$$y_i = c + \beta x_{i-j} + \varepsilon \quad (8)$$

where c and β are coefficients of the linear model; x is the index value (NAO, IOD) (independent variable); y is the precipitation value for each meteorology stations (Bodrum, Igdir) (dependent value); j is the phase shift in months; j = 0, 1, 2, . . . , 9, 10 values were used in this study.

The determination coefficient (R^2) and Akaike information criterion (AIC) values were used as performance criteria for the linear models. Higher R^2 and lower AIC values indicate a strong relationship between dependent and independent variables. According to different phase shift values, R^2 and AIC values were obtained (Table 3). After the cross-spectral analysis, the phase shift was calculated as 7.67 months between monthly total precipitations measured at the Bodrum meteorology station and the NAO index for the 22-month period. In the statistical analysis, the highest relationship was observed at the 7-month phase shift mark for Bodrum and the NAO models, as expected. Thus, the highest R^2 value is 0.994 and the lowest AIC value is −17.240 (bold in the Table 3) for Bodrum-NAO at the 7-month phase shift mark. A similar process was applied to the IOD index and Igdir precipitation values for the 20-month period. The phase shift was calculated as 4.33 months for this period, and as expected the highest relationship was observed at the 4-month phase shift. The highest R^2 value was 0.918 and lowest AIC value was −8.596 for Igdir-IOD at the 4-month phase shift (bold in the Table 3, Figure 17).

Table 3. The R^2 and Akaike information criterion (AIC) values for Bodrum-NAO and Igdir-IOD (Bold values indicate highest relationship).

	Bodrum-NAO		**Igdir-IOD**	
Phase Shift (Months)	R^2	**AIC**	R^2	**AIC**
0	0.204	−12.323	0.114	−6.223
1	0.035	−12.130	0.360	−6.547
2	0.009	−12.103	0.644	−7.132
3	0.133	−12.237	0.857	−8.045
4	0.369	−12.557	**0.918**	**−8.596**
5	0.646	−13.137	0.802	−7.719
6	0.879	−14.208	0.555	−6.908
7	**0.994**	**−17.240**	0.271	−6.414
8	0.957	−15.246	0.060	−6.158
9	0.778	−13.608	0.003	−6.097
10	0.514	−12.822	0.120	−6.220

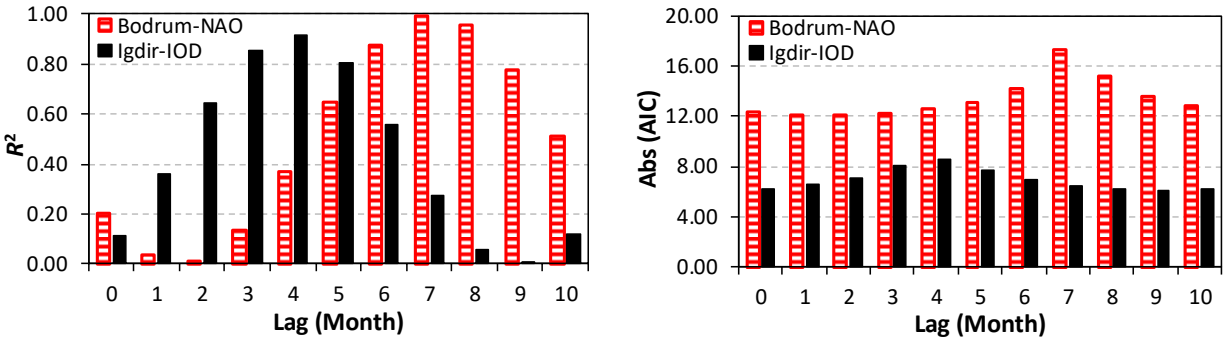

Figure 17. Results of statistical analysis of Bodrum-NAO and Igdir-IOD.

4. Conclusions

This paper focuses on the effects of the different teleconnection patterns, namely the NAO and IOD indices, on precipitation in Turkey. For this purpose, 239 different meteorology stations were considered, then cross-spectral analysis were performed between the indices and precipitation values. The remarkable results from this study can be summarized as follows:

- The phase shift (Figure 15) and cross-power spectral density (CPSD) (Figure 16) clusters are not consistent with the rainfall regions (Figure 1) and climate regions (Figure 2) in Turkey. Phase shift and CPSD clusters move in an east–west direction according to the period;
- According to the cross-spectral analysis results, phase shift and CPSD values between the NAO and meteorology stations were mostly clustered in the west of Turkey for the 22–23-month period. This means that the stronger relationships were observed in the west because the NAO is closer to west of Turkey. Similarly, phase shift and CPSD values between the IOD and meteorology stations were clustered for the 20–21-month period in the east and southeast of Turkey. Accordingly, the stronger relationships were observed in the east because the IOD is closer to east of Turkey. Therefore, Bodrum meteorology station in the west and Igdir meteorology station in the east were examined as examples in this study according to the strong relationships with the NAO and the IOD indices, respectively, for the above periods. Moreover, NAO2223 and IOD2021 showed strong relationships with western and eastern meteorology stations, respectively, in close periods (20–21 months and 22–23 months);
- The phase shift was calculated as 7.67 months for Bodrum-NAO in the 22-month period and as 4.33 months for Igdir-IOD in the 20-month period by cross-spectral analysis. These results indicate that the effect of the NAO is seen after 7.67 months in Bodrum meteorology station precipitation data and the effect of the IOD is seen after 4.33 months in Igdir meteorology station precipitation data. According to different phase shift values, the R^2 and AIC values were obtained. Higher R^2 and lower AIC values indicate a strong relationship between dependent and independent variables. After the linear modeling undertaken to statistically check the accuracy of the above values, the highest R^2 (0.994 for Bodrum-NAO, 0.918 for Igdir-IOD) and lowest AIC (-17.240 for Bodrum-NAO, -8.596 for Igdir-IOD) values of the model were obtained at the 7-month phase shift point for Bodrum-NAO and at the 4-month phase shift point for Igdir-IOD. Thus, the phase shift values obtained for relevant period after the cross-spectral analysis were statistically verified;
- The NAO and the IOD indices can be used in precipitation forecast studies in western and eastern Turkey, respectively.

In the next study, prediction models will be created using the relationships obtained. The calculations should be made for a certain period; since the power is higher in longer periods, the periods used should be as long as possible. Both ocean oscillation and precipitation data (signals) are superpositions of sine waves with different periods. Therefore,

the original precipitation and index data should be used in the model after a reasonable band-pass filter has been applied for the studied frequency, while the phase shift in the relevant period should be considered.

Author Contributions: Conceptualization, U.S.D. and A.C.K.; methodology, U.S.D. and A.C.K.; software, U.S.D. and A.C.K.; validation, U.S.D. and A.C.K.; formal analysis, U.S.D. and A.C.K.; investigation, U.S.D. and A.C.K.; resources, U.S.D. and A.C.K.; data curation, U.S.D. and A.C.K.; writing—original draft preparation, U.S.D. and A.C.K.; writing—review and editing, U.S.D. and A.C.K.; visualization, U.S.D. and A.C.K.; supervision, A.C.K. All authors have read and agreed to the published version of the manuscript.

Funding: This research received no external funding.

Institutional Review Board Statement: Not applicable.

Informed Consent Statement: Not applicable.

Data Availability Statement: Not applicable.

Acknowledgments: The authors of this article would like to thank the Turkish State Meteorological Service for the precipitation data. The authors extend their thanks to James W. Hurrell and National Oceanic and Atmospheric Administration (NOAA) for providing the NAO and the IOD data used in the study. The authors also would like to thank the three anonymous reviewer for his/her suggestions and comments.

Conflicts of Interest: The authors declare no conflict of interest.

References

1. Durkee, J.D.; Frye, J.D.; Fuhrmann, C.M.; Lacke, M.C.; Jeong, H.G.; Mote, T.L. Effects of the North Atlantic Oscillation on precipitation-type frequency and distribution in the eastern United States. *Theor. Appl. Climatol.* **2008**, *94*, 51–65. [CrossRef]
2. Hurrell, J.W. North Atlantic climate variability: The role of the North Atlantic Oscillation. *J. Mar. Syst.* **2010**, *79*, 231–244. [CrossRef]
3. Walker, G.T. Correlation in seasonal variations of weather IX: A further study of world weather. *Mem. India Met. Dept.* **1924**, *24*, 275–332.
4. Walker, G.T.; Bliss, E.W. Memoirs of the Royal Meteorological Society. *Q. J. R. Meteorol. Soc.* **1932**, *4*, 53–84.
5. Wallace, J.M. North Atlantic Oscillation/annular mode: Two paradigms one phenomenon. *Q. J. R. Meteorol. Soc.* **2000**, *126*, 791–805. [CrossRef]
6. Hurrell, J.W. Decadal trends in the North Atlantic Oscillation, regional temperatures and precipitation. *Science* **1995**, *269*, 676–679.
7. Hurrell, J.W.; Kushnir, Y.; Visbeck, M.; Ottersen, G. An overview of the North Atlantic Oscillation. *Geophys. Monogr.* **2003**, *134*, 1–35. [CrossRef]
8. Wibig, J. Precipitation in Europe in relation to circulation patterns at the 500 hPa level. *Int. J. Climatol.* **1999**, *19*, 253–269. [CrossRef]
9. Tatlı, H.; Menteş, Ş.S. Detrended cross-correlation patterns between North Atlantic oscillation and precipitation. *Theor. Appl. Climatol.* **2019**, *138*, 387–397. [CrossRef]
10. Hurrell, J.W.; Van, L.H. Decadal variations in climate associated with the North Atlantic oscillation. *Clim. Chang.* **1997**, *36*, 301–326. [CrossRef]
11. Vergni, L.; Lena, B.D.; Chiaudani, A. Statistical characterization of winter precipitation in the Abruzzo region (Italy) in relation to the North Atlantic Oscillation (NAO). *Atmos. Res.* **2016**, *178–179*, 279–290. [CrossRef]
12. Zamrane, Z.; Turki, I.; Laignel, B.; Mahé, G.; Laftouhi, N.E. Characterization of the interannual variability of precipitation and streamflow in Tensift and Ksob basins (Morocco) and links with the NAO. *Atmosphere* **2016**, *7*, 84. [CrossRef]
13. Castro, A.; Vidal, M.I.; Calvo, A.I.; Fernández, R.M.; Fraile, R. May the NAO index be used to forecast rain in Spain? *Atmosfera* **2011**, *24*, 251–265.
14. Garcia, N.O.; Gimeno, L.; Torre, D.L.L.; Nieto, R.; Añel, J.A. North Atlantic Oscillation (NAO) and precipitation in Galicia (Spain). *Atmosfera* **2005**, *18*, 25–32.
15. Massei, N.; Durand, A.; Deloffre, J.; Dupont, J.P.; Valdes, D.; Laignel, B. Investigating possible links between the North Atlantic Oscillation and precipitation variability in Northwestern France over the past 35 years. *J. Geophys. Res.* **2007**, *112*, D09121. [CrossRef]
16. Hermida, L.; López, L.; Merino, A.; Berthet, C.; García, O.E.; Sánchez, J.L.; Dessens, J. Hailfall in southwest France: Relationship with precipitation, trends and wavelet analysis. *Atmos. Res.* **2015**, *156*, 174–188. [CrossRef]
17. Saunders, M.A.; Qian, B. Seasonal predictability of the winter NAO from North Atlantic sea surface temperatures. *Geophys. Res. Lett.* **2002**, *29*, 1–6. [CrossRef]
18. Eshel, G. Forecasting the North Atlantic Oscillation using North Pacific surface pressure. *Mon. Weather Rev.* **2003**, *131*, 1018–1025. [CrossRef]

19. Wang, L.; Ting, M.; Kushner, P.J. A robust empirical seasonal prediction of winter NAO and surface climate. *Sci. Rep.* **2017**, *7*, 279. [CrossRef]
20. Dobrynin, M.; Domeisen, D.I.V.; Müller, W.A.; Bell, L.; Brune, S.; Bunzel, F.; Düsterhus, A.; Fröhlich, K.; Pohlmann, H.; Baehr, J. Improved teleconnection based dynamical seasonal predictions of boreal winter. *Geophys. Res. Lett.* **2018**, *45*, 3605–3614. [CrossRef]
21. Chlaściak, Ś.M.; Niedzielski, T. Forecasting the North Atlantic Oscillation index using altimetric sea level anomalies. *Acta Geod. Geophys.* **2020**, *55*, 531–553. [CrossRef]
22. Saji, N.H.; Goswami, B.N.; Vinayachandran, P.N.; Yamagata, T. A dipole mode in the tropical Indian Ocean. *Nature* **1999**, *401*, 360–363. [CrossRef] [PubMed]
23. Saji, N.H.; Yamagata, T. Possible impacts of Indian Ocean Dipole mode events on global climate. *Clim. Res.* **2003**, *25*, 151–169. [CrossRef]
24. Clark, C.O.; Webster, P.J.; Cole, J.E. Interdecadal variability of the relationship between the Indian Ocean zonal mode and East African coastal rainfall anomalies. *J. Clim.* **2003**, *16*, 548–554. [CrossRef]
25. Dubache, G.; Ogwang, B.A.; Ongoma, V.; Islam, A.R.M.T. The effect of Indian Ocean on Ethiopian seasonal rainfall. *Meteorol. Atmos. Phys.* **2019**, *131*, 1753–1761. [CrossRef]
26. Guan, Z.; Ashok, K.; Yamagata, T. Summertime response of the tropical atmosphere to the Indian Ocean sea surface temperature anomalies. *J. Meteorol. Soc. Jpn.* **2003**, *81*, 533–561. [CrossRef]
27. Yuan, Y.; Yang, H.; Zhouc, W.; Li, C. Influences of the Indian Ocean dipole on the Asian summer monsoon in the following year. *Int. J. Climatol.* **2008**, *28*, 1849–1859. [CrossRef]
28. Hussain, M.S.; Kim, S.; Lee, S. On the relationship between Indian Ocean Dipole events and the precipitation of Pakistan. *Theor. Appl. Climatol.* **2016**, *130*, 673–685. [CrossRef]
29. Saji, N.H.; Ambrizzi, T.; Ferraz, S.E.T. Indian Ocean Dipole mode events and austral surface air temperature anomalies. *Dyn. Atmos. Ocean.* **2005**, *39*, 87–101. [CrossRef]
30. Hardiman, S.C.; Dunstone, N.J.; Scaife, A.A.; Smith, D.M.; Knight, J.R.; Davies, P.; Claus, M.; Greatbatch, R.J. Predictability of European winter 2019/20: Indian Ocean dipole impacts on the NAO. *Atmos. Sci. Lett.* **2020**, 1–10. [CrossRef]
31. Chan, S.C.; Behera, S.K.; Yamagata, T. Indian Ocean Dipole influence on South American rainfall. *Geophys. Res. Lett.* **2008**, *35*, L14S12. [CrossRef]
32. Sariş, F.; Hannah, D.M.; Eastwood, W.J. Spatial variability of precipitation regimes over Turkey. *Hydrol. Sci. J.* **2010**, *55*, 234–249. [CrossRef]
33. Türkeş, M.; Erlat, E. Climatological responses of winter precipitation in Turkey to variability of the North Atlantic Oscillation during the period 1930–2001. *Theor. Appl. Climatol.* **2005**, *81*, 45–69. [CrossRef]
34. Türkeş, M.; Erlat, E. Precipitation changes and variability in Turkey linked to the north atlantic oscillation during the period 1930–2000. *Int. J. Climatol.* **2003**, *23*, 1771–1796. [CrossRef]
35. Türkeş, M.; Erlat, E. Winter mean temperature variability in Turkey associated with the North Atlantic Oscillation. *Meteorol. Atmos. Phys.* **2009**, *105*, 211–225. [CrossRef]
36. Küçük, M.; Kahya, E.; Cengiz, T.M.; Karaca, M. North Atlantic Oscillation influences on Turkish lake levels. *Hydrol. Process* **2009**, *23*, 893–906. [CrossRef]
37. Kahya, E. The Impacts of NAO on the hydrology of the Eastern Mediterranean. *Adv. Glob. Chang. Res.* **2011**, *46*, 57–71. [CrossRef]
38. Bozyurt, O.; Özdemir, M.A. The relations between North Atlantic Oscillation and minimum temperature in Turkey. *Procedia Soc. Behav. Sci.* **2014**, *120*, 532–537. [CrossRef]
39. Sönmez, İ.; Kömüşcü, A.Ü. Reclassification of rainfall regions of Turkey by K-means methodology and their temporal variability in relation to North Atlantic Oscillation (NAO) . *Theor. Appl. Climatol.* **2011**, *106*, 499–510. [CrossRef]
40. Baltacı, H.; Akkoyunlu, B.O.; Tayanç, M. Relationships between teleconnection patterns and Turkish climatic extremes. *Theor. Appl. Climatol.* **2018**, *134*, 1365–1386. [CrossRef]
41. Baltaci, H.; Arslan, H.; Akkoyunlu, B.O.; Gomes, H.B. Long-term variability and trends of extended winter snowfall in Turkey and the role of teleconnection patterns. *Meteorol. Appl.* **2020**, *27*, e1891. [CrossRef]
42. Yılmaz, E.; Çiçek, İ. Detailed Köppen-Geiger climate regions of Turkey. *Int. J. Hum. Sci.* **2018**, *15*, 225–242. (In Turkish) [CrossRef]
43. Jones, P.D.; Jonsson, T.; Wheeler, D. Extension to the North Atlantic Oscillation using early instrumental pressure observations from Gibraltar and south-west Iceland. *Int. J. Climatol.* **1997**, *17*, 1433–1450.
44. ClimateDataGuide. Available online: https://climatedataguide.ucar.edu/climate-data/hurrell-north-atlantic-oscillation-theNAO-index-station-based.climatedataguide.ucar.edu (accessed on 12 September 2019).
45. NOAA. Available online: https://psl.noaa.gov/gcos_wgsp/Timeseries/Data/dmi.long.data (accessed on 12 September 2019).
46. Blackman, R.B.; Tukey, J.W. The Measurement of Power Spectra. *Bell Syst. Tech.* **1958**, *37*, 185. [CrossRef]
47. Trauth, M.H. *MATLAB Recipes for Earth Sciences Fourth Edition 2014*; Springer: Berlin/Heidelberg, Germany, 2014.
48. Kutzbach, J.E.; Bryson, R.A. Variance spectrum of Holocene climatic fluctuations in the north Atlantic sector. *J. Atmos. Sci.* **1974**, *31*, 1958–1963. [CrossRef]
49. Allen, M.R. Interactions between the Atmosphere and Oceans on Time-Scales of Weeks to Years. Ph.D. Thesis, University of Oxford, Oxford, UK, 1992.

50. Allen, M.R.; Smith, L.A. Investigating the Origins and Significance of Low-Frequency Modes of Climate Variability. *Geophys. Res. Lett.* **1994**, *21*, 883–886. [CrossRef]
51. Gilman, D.L.; Fuglister, F.J.; Mitchell, J.M., Jr. On the Power Spectrum of "Red Noise". *J. Atmos. Sci.* **1963**, *20*, 182–184.
52. Mann, M.E.; Lees, J.M. Robust estimation of background noise and signal detection in climatic time series. *Clim. Chang.* **1996**, *33*, 409–445. [CrossRef]
53. Matyasovszky, I. Estimating red noise spectra of climatological time series. *Idoejaras* **2013**, *117*, 187–200.
54. Ghil, M.; Allen, M.R.; Dettinger, M.D.; Ide, K.; Kondrashov, D.; Mann, M.E.; Robertson, A.W.; Saunders, A.; Tian, Y.; Varadi, F.; et al. Advanced spectral methods for climatic time series. *Rev. Geophys.* **2002**, *40*, 1–41. [CrossRef]
55. Dickey, D.A.; Fuller, W.A. Distribution of the estimators for autoregressive time series with a unit root. *J. Am. Stat. Assoc.* **1979**, *74*, 427–431. [CrossRef]